Desalination and Water Treatment
www.deswater.com

doi: 10.5004/dwt.2017.21358

90 (2017) 299–310
September

Comparative analysis of adsorption and light decomposition of methylene blue by ordered mesoporous C-Nb-TiO_2 nanocomposites prepared via self-assembly and sol–gel methods

Ying Ding, Jianzhong Zhu*, Di Zhang, Shengtao Jiang, Khan Osama Sarwar, Shenglu Chen

Key Laboratory for Integrated Regulation and Resource Development on Shallow Lake of Ministry of Education, College of Environment, Hohai University, Nanjing 210098, China, Tel. +86 13739186298; email: zhuhhai2010@hhu.edu.cn (J. Zhu), Tel. +86 18751958626; email: dingying19900123@163.com (Y. Ding), Tel. +86 18805158912; email: 6486863352@qq.com (D. Zhang), Tel. +86 13626682900; email: 570404482@qq.com (S. Jiang), Tel. +86 15295527036; email: 1964073589@qq.com (K. Osama), Tel. +86 15295512755; email: 1324425971@qq.com (S. Chen)

Received 16 March 2017; Accepted 22 August 2017

ABSTRACT

Highly ordered mesoporous carbon–niobium doped TiO_2 nanocomposites with nanocrystal frameworks have been synthesized via the self-assembly and sol–gel methods from organic–inorganic–amphiphilic co-assembly followed by the in situ crystallization technology. A soluble resol polymer was used as a carbon precursor, TiO_2 as an inorganic precursor, and triblock copolymer F127 as a template. The soluble resol–niobium doped TiO_2 nanocomposites with controllable texture properties and composition can be obtained in a wide range from 0.0 to 20.0 wt% TiO_2 by adjusting the initial mass ratios. A detailed characterization of the nanocomposites shows that films contain nanoparticles with the anatase modification with pentavalent Nb chloride dissolved into the anatase and mesoporous carbon structure. The nanocomposites have high surface area (424–613 $m^2\ g^{-1}$) and ordered pore size (~3.9 nm). Both energy-dispersive X-ray and X-ray fluorescence data detected the presence of Nb and TiO_2 in composite mesoporous materials. The scanning electron and transmission electron microscopic images of C-niobium doped TiO_2 nanocomposites exhibit highly ordered two dimensional hexagonal mesostructure. The Nb-doped films displayed an enhanced visible light absorption with a red-shift of the optical absorption edge and X-ray diffraction data showed that the films consisted of the anatase polymorph of TiO_2. Ultraviolet–visible spectrophotometry data showed that the optical indirect band gap of the films decreased significantly, from 3.13 eV (undoped) to 3.04 eV (0.2 mol% Nb). X-ray photoelectron spectroscopic results of materials show that the characteristic peaks at C1s, Ti2p, O1s and Nb3d exhibit the existence of C, Ti, O, Nb in nanocomposites. Additionally, the nanocomposites show good performance in the degradation of methylene blue due to the photocatalytic activity of the Nb-doped TiO_2 nanocrystals and the strong adsorptive capacity of the mesoporous carbon.

Keywords: Mesoporous carbon; Titanium dioxide; Nb-doping; Adsorption; Light decomposition

1. Introduction

Dyeing wastewater, such as methylene blue, rhodamine B, reactive brilliant red are widely used in industrial processes and domestic activities, leading to water pollution [1–3]. Among this dyeing wastewater, methylene blue wastewater has become one of the largest production in industrial waste water [4]. At the same time, methylene blue has highly toxic and carcinogenic properties and has potential harm to human body. Animals exposed to methylene blue may have

* Corresponding author.

some toxic conditions such as low body temperature, acidosis, hypercapnia, corneal damage, conjunctival damage and the formation of Heinz bodies [5,6]. Because of the complexity of the molecular structure of dyestuff, the degradation of dyestuff has not been effectively removed. Methylene blue is one of the hard-degradable organic compounds removed from dyeing wastewater [7,8].

Among the technologies used for the treatment of dyeing wastewater such as adsorption [9], the light decomposition using TiO_2 as a photocatalyst is considered to be a promising technology for the degradation of the hard-degradable organic compounds in environment cleaning since it has many advantages over conventional other techniques [10,11]. Titanium dioxide photocatalysis has been a promising technology for water remediation such as dyeing wastewater in the past recent decades [12]. TiO_2 has been most widely used to remove different chemical pollutants from drinking water and waste water among the various photocatalysts investigated so far [13–16].

One of the most effective techniques for modification of the TiO_2 band gap is doping with transition metals [17]. TiO_2-doped transition metals are suitable for destruction of various organic compounds at even low concentrations, due to its chemical stability, non-toxicity optical and electronic properties [18]. Recent research has been carried out on the use of several dopants such as Co [19], Fe [20], Mn [21], and Nb. In the preceding dopants, Nb has attracted strong interest owing to valence and size effects. In the present paper, we explore the potential of using Nb-doped TiO_2 as a visible active photocatalytic material [22–24].

An alternative method is to add amorphous components, such as phosphoxides or carbon into the mesostructured TiO_2 framework so it can form a glasslike phase. Recent researchers are involved in the preparation of graphene or carbon nanotube [25–28], but few researches study mesoporous materials especially to deliver a synergistic effect. The unique and fascinating properties of mesoporous carbon such as large surface area, uniform pore size distribution, functionalizable surfaces, strong UV absorption, and surface enhanced Raman scattering make them one of the most promising materials for adsorption of pollutants, tissue engineering as well as electronics [29]. Mesoporous carbon is a very reliable material for fabricating photocatalytic material containing inorganic composites because of its unique electronic property, ordered structure, high transparency, and large theoretical specific surface area, etc. [30–34]. Recently, many nanomaterials based photocatalysts have been reported indicating that coupling TiO_2 with nanomaterials such as graphene and carbon nanotube can lead to enhanced electronic and photocatalytic properties of TiO_2 [35]. Mesoporous carbon can decrease the recombination of electron–hole pairs, enhancing surface adsorbed amount of organic pollutants [32,36,37]. It suggests that the mesoporous carbon phase prevents the growth of nanocrystals and improves the stability of the mesostructure. Herein, we demonstrate self-assembly and sol–gel methods respectively to fabricate mesoporous carbon-niobium doped TiO_2 nanocomposites by using resols as an organic precursor, $Ti(OBu)_4$ as an inorganic precursor, $NbCl_5$ as a doping material and amphiphilic triblock copolymer F127 as a template.

Methylene blue dye has been chosen as a probe to study photocatalytic performance of mesoporous carbon–niobium doped TiO_2 nanocomposites. In a recent study, Zhang et al. [34] reported the photocatalyst of P25 for the degradation of rhodamine B. In their work, anatase phase TiO_2 appears to be photocatalytically more active than that in rutile phase. Hence, it is necessary to evaluate the effect of coupling of anatase TiO_2 nanoparticles with mesoporous carbon towards photocatalytic degradation of dyes [37]. Consequently, it is necessary to increase the service life of the niobium-doped TiO_2 and enhance its photocatalytic activity.

In this study, the mesoporous carbon–niobium doped TiO_2 nanocomposites were prepared via self-assembly and sol–gel methods. Different types of characterization were utilized to characterize the composition, structure and surface activity of the C-Nb doped TiO_2 nanocomposites. The adsorption and photocatalytic degradation performance of dye wastewater were systematically studied with prepared water in laboratory. The concentration of methylene blue as well as the degraded water samples was analyzed by UV to evaluate the adsorption and photocatalytic degradation efficiency. The main objectives of this work were (1) to investigate the extension effect of Nb-doped TiO_2 nanocomposite about the optical absorption into the visible and utilize a larger portion of the sunlight; (2) to measure the adsorption and photocatalytic degradation performance of the mesoporous carbon–niobium doped TiO_2 nanocomposite; (3) to compare the properties of the nanocomposites prepared via two synthetic methods which is self-assembly and sol–gel methods.

2. Materials and experimental

2.1. Materials

The triblock copolymer Pluronic F127 and formaldehyde solution (36.5–38.0 wt%) were obtained from Sigma-Aldrich. Tetrabutyl titanate, niobium pentachloride, glacial acetic acid (>98% purity) were purchased from Nanjing Chemical Reagent Co., Ltd. (Nanjing, China). In addition, AR grade ethanol, methylene blue, phenol, HCl, NaOH all were purchased from Chemical Co., Ltd. (Nanjing, China). All these materials were used without further purification.

2.2. Nanocomposites preparation

Mesoporous carbon was prepared with the preformed phenolic resin resol solution as a carbon resource, and triblock copolymer F127 as templates in an ethanol solution according to our previous report [38,39] and other literatures [36]. The mesoporous carbon–niobium doped TiO_2 nanocomposites were prepared via self-assembly method: 3.5 g of $Ti(OBu)_4$ was rapidly added dropwise to a clear solution containing 2.0 mL of concentrated HCl, 2.49 g of HAc, 2.6 g of F127 and 23 g of EtOH. Then, 0.0067 g of $NbCl_5$ solids was slowly added into the solution and followed by vigorous stirring of the mixture for 1 h. As soon as 5.0 g of 20 wt% resols ethanolic solution was added, the solution rapidly became nacarat and was stirred for additional 10 min. The resulting homogeneous solution was poured into a porcelain dish. The porcelain dish was placed in an oven at 40°C and the ethanol was volatilized for 8 h without any humidity control. The temperature was then raised to 100°C for 24 h. The resulting film was scraped from the

porcelain plate and ground into a powder. Then, it is placed in a tube furnace under the protection of nitrogen at 500°C for 3 h. The final product was identified as NTC1-a, where a represents the mass ratio of resols ethanolic to tetrabutyl titanate during the preparation. The nanocomposites containing 1.75, 3.5, 7.0 and 14.0 wt% resols ethanolic were denoted as NTC1-1.75, NTC1-3.5, NTC1-7, and NTC1-14, respectively.

The mesoporous carbon–niobium doped TiO_2 nanocomposites were prepared via sol–gel method: First, we weighed 1.0 g of mesoporous carbon into 20 mL of anhydrous ethanol and then added 0.35 mL of deionized water to the solution, recorded as A solution. Then take 5.0 g of tetrabutyl titanate dropwise under stirring to 10 mL of absolute ethanol followed by the addition of 0.05 mL of glacial acetic acid and 0.10 mL of concentrated hydrochloric acid as the hydrolysis inhibitor. The pH of the solution was controlled at about 2–3 and then 0.0096 g of niobium pentachloride was quickly added to the solution (to avoid deliquescence). Then, Nb-TiO_2 sol was obtained after reacting for 1 h at room temperature under magnetic stirring, recorded as B solution. After that we put the A solution into the ultrasonic cleaner for ultrasonic dispersion treatment for 1 h and then A liquid was added to the B solution under the rapid stirring, followed by ultrasonic dispersion treatment for 60 min. The mixture has formed a uniform gel at this time, hence, make it aging for 10 h. Then the gel was dried at 80°C in a thermostatic vacuum oven and washed twice with deionized water. After drying again, the material was placed in a tubular resistance furnace and calcined at a constant temperature of 500°C in a nitrogen atmosphere for 3 h, then cooled it to room temperature. At last the mesoporous carbon–niobium doped TiO_2 nanocomposites were obtained. By changing the mass of mesoporous carbon, a composite material with different carbon content can be prepared, denoted as NTC2-*b*, where *b* is the theoretical mass fraction of mesoporous carbon in the material. The appropriate amount of mesoporous carbon was used to achieve the loading of 0.0, 5.0, 10.0, 15.0 or 20.0 wt% mesoporous carbon on TiO_2 to make nanocomposites. The nanocomposites containing 0.0, 5.0, 10.0, 15.0 and 20.0 wt% mesoporous carbon were denoted as NTC2-0, NTC2-5, NTC2-10, NTC2-15 and NTC2-20, respectively.

2.3. Nanocomposites characterization

The surface area and the porosity of the nanocomposites were determined using an ASAP2020 surface area analyzer and the nitrogen sorption method. Nitrogen adsorption–desorption isotherms were plotted as relative pressure (p/p_0) vs. adsorbed gas volume. The pore width distributions and pore volumes were determined from the adsorption part of the isotherm by using the Brunauer–Emmett–Teller (BET) method [40]. X-ray fluorescence (XRF) and energy-dispersive X-ray (EDX) were used to analyze whether TiO_2 and Nb were successfully doped into mesoporous carbon composites. Scanning electron microscopy (SEM S-3400N) and transmission electron microscope (TEM JEM-2010) were used to image the mesoporous structures in the nanocomposites samples. X-ray diffractograms of the prepared NTC1-3.5 and NTC2-15 nanocomposites were recorded on a D/max-2500/PC with Cu Ka radiation (λ = 1.5418 Å). The obtained X-ray diffraction (XRD) patterns were compared with JCPDSs (Joint Committee on Powder Diffraction Standards) cards. The surface of the sample was analyzed by the PHI5000 VersaProbe photoelectron spectrometer from ULVAC-PHI Co. Ltd. and the chemical valence state and the bonding state of the element were determined by the position of element binding energy. X-ray photoelectron spectroscopy (XPS) was used to determine the chemical valence and molecular structure of elements. In addition, the wavelength range of light absorption of the material before and after the modification was tested by using the Shimadzu UV-2401PC type UV–visible spectrophotometer. The samples were powdered with a resolution of 0.5 nm, a scanning rate of 40 nm/min and a scanning range of 200–800 nm.

2.4. Photocatalytic activity measurement

The photodegradation of the dye methylene blue was carried out in a self-made photocatalytic reactor. Nanocomposites (0.5 g) was magnetically stirred in a mixed solution, which contains 500 mL of methylene blue with an initial concentration of 50 mg/L, in the darkness for at least 6 h to reach the adsorption equilibrium of methylene blue with the nanocomposites. The solution was irradiated by a 25 W mercury lamp, which was placed in the middle of the container irradiation cell made of quartz. The degradation rate was determined at every 30 min intervals by UV–Vis absorption. Fig. 1 shows the photocatalytic reactor setup that was used to evaluate efficiency of prepared nanocomposites.

3. Results and discussion

3.1. Brunauer–Emmett–Teller tests

The N_2 adsorption and desorption isotherms of the NTC1-3.5 and NTC2-15 nanocomposites studied in this work are plotted in Fig. 2, and the corresponding pore

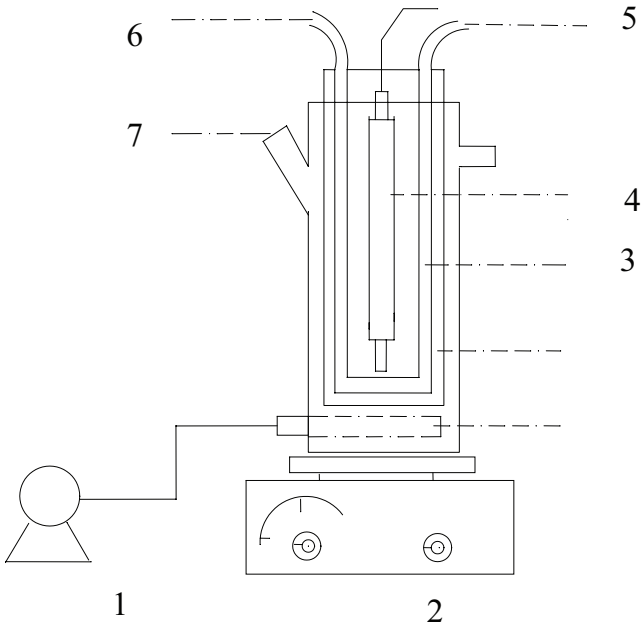

Fig. 1. Schematic diagram of photocatalytic reactor. (1) aeration pump; (2) magnetic stirrer; (3) condensate; (4) UV lamp; (5) condensate outlet; (6) condensate inlet; (7) sampling port.

diameter distributions calculated from the desorption isotherm branches are shown in Fig. 3. All the nanocomposites exhibit representative type IV isotherms and the absorption and desorption curves of NTC1-3.5 and NTC2-15 nanocomposites exhibited H_2 type hysteresis loops, which indicated that the pore structure of the nanocomposites had two-dimensional hexagonal pore structure. It is related to two-dimensional hexagonal pore structure, presumably driven by the growth of anatase niobium-doped TiO_2 within the pore walls. Some of large TiO_2 nanocrystals can thrust into the channels and block the mesopores, which results in a two-dimensional hexagonal pore structure and H_2 type hysteresis loop. A very sharp pore size distribution at a mean value of 3.5–3.9 nm was calculated from the adsorption branch on the basis of Barrett-Joyner-Halenda (BJH) model.

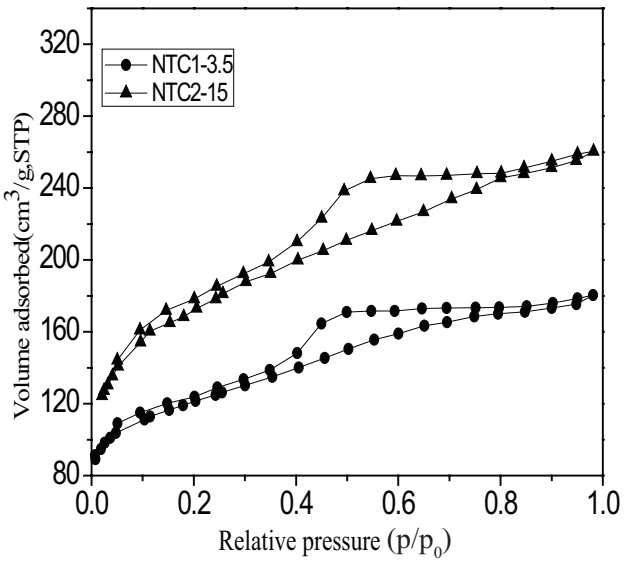

Fig. 2. N_2 adsorption/desorption isotherms of NTC1-3.5 and NTC2-15 nanocomposites.

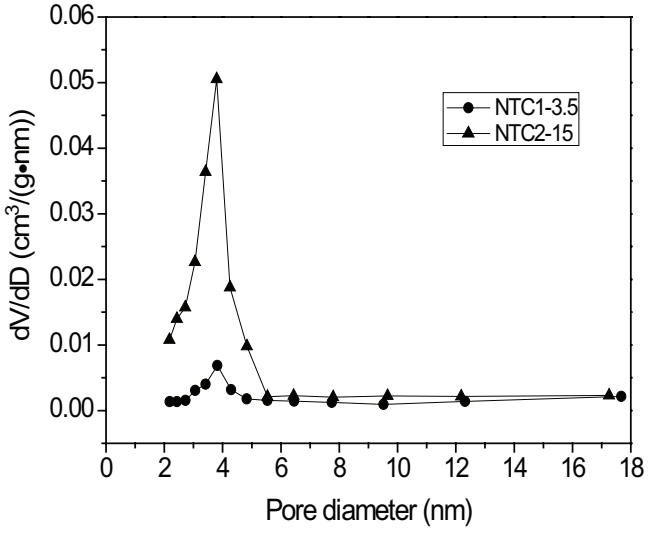

Fig. 3. Pore size distributions of NTC1-3.5 and NTC2-15 nanocomposites.

Nitrogen adsorption–desorption isotherms were plotted as relative pressure (p/p_0) vs. adsorbed gas volume. The pore width distributions and pore volumes were determined from the adsorption part of the isotherm by using the BET method. The Kelvin equation (1) was used in our calculations of pore size distributions:

$$r(p/p_0) = \frac{2\gamma V_L}{RT\ln[(p_0/p)]} \quad (1)$$

where V_L is the molar volume of the liquid adsorbate, γ is its surface tension, R is the universal gas constant, and T is the absolute temperature. The pore volumes were assessed from the adsorption isotherm $V(p/p_0)$ for a given sample by subtracting the amount adsorbed on its external surface:

$$V_P(p/p_0) = V(p/p_0) - \frac{S_{ex}}{S_{BET,ref}} V_{ref}(p/p_0) \quad (2)$$

In Eq. (2), $S_{BET,ref}$ and $V_{ref}(p/p_0)$ are the BET-specific surface area and the adsorption isotherm, respectively, for the reference adsorbent used in calculations of the external surface area S_{ex}. The calculation results are shown in Table 1.

Comparing the materials prepared by two different synthesis methods, we can see that the pore size of NTC2-15 concentrates around 3.9 nm, indicating that the sample has a more uniform pore structure rather than a chaotic pore structure. The pore size distribution of sample NTC1-3.5 is not obvious, but it is also about 3.5 nm. This may be due to the formation of the mesoporous carbon, which is blocked by the titanium dioxide particles during the synthesis of nanocomposites via the self-assembly method. In the preparation of nanocomposites by sol–gel method, we added the synthesized mesoporous carbon in to the gel solution. The main properties of the nanocomposites including BET-specific surface areas, average pore diameters and pore volumes are listed in Table 1.

3.2. EDX and XRF analysis

In this paper, the synthesis of C-Nb-TiO_2 composite materials (NTC1-3.5 and NTC2-15) was analyzed by EDX that showed various element types of the composition and proportion and XRF that showed the content of Nb and TiO_2 composite material, respectively. We selected five points in the sample to be detected and the average content of them was listed in the following table. From Table 2, it can be seen that the carbon and oxygen elements in NTC1-3.5 are relatively large and

Table 1
The main properties of the NTC1-3.5 and NTC2-15 nanocomposites

Samples	NTC1-3.5	NTC2-15
BET surface area (m^2/g)	424	604
Micropore area (m^2/g)	361	528
Pore volume (cm^3/g)	0.2944	0.4509
Micropore volume (cm^3/g)	0.1422	0.2063
Pore size (nm)	3.5	3.9

the proportion of Ti and Nb is 6.38% and 0.09%, respectively. Similarly, the proportion of carbon and oxygen in NTC2-15 is larger and the proportion of Ti and Nb is 14.28% and 0.15%, respectively, which content was similar to that of XPS.

From Table 3, it can be seen that the proportion of TiO_2 in NTC1-3.5 and NTC2-15 are 25.43% and 40.52% relatively. NTC2-15 showed high proportion of TiO_2 and the proportion of carbon is lower than NTC1-3.5 which caused the photocatalytic ability of NTC1-3.5 composite weak and the adsorption capacity is stronger and the photocatalytic activity of NTC2-15 composite is improved obviously.

3.3. SEM and TEM tests

From Fig. 4, it can be seen that the particle size of TiO_2 is very large after the particles of NTC2-15 are sintered at high temperature, which are obviously bonded and the agglomeration with the mesoporous carbon particles. The main reason is that the titanium dioxide particles still be agglomerated locally after sintering at high temperature even if the Nb-TiO_2 sol–gel was evenly loaded on the surface of the mesoporous carbon material when we prepare the mesoporous carbon–niobium doped TiO_2 nanocomposites under ultrasonic treatment. We can also observe that the proportion of titanium dioxide in nanocomposites is larger. In Fig. 4(a), the particle size of TiO_2 supported on the mesoporous carbon is about 15–20 nm and the range of size distribution of the particles is small. For the NTC1-3.5 composites, the proportion of mesoporous carbon is larger and the TiO_2 particles are evenly distributed in the pores of the mesoporous carbon. The stripe structure on the surface of the material can be seen through the SEM image (Fig. 4(b)), which showed the appearance of mesopores. From the images, it can be seen that the nanocomposites surface is relatively smooth and the niobium-doped TiO_2 particles are wrapped in the channel of mesoporous carbon.

The nanocomposites structure is relatively uniform because Nb-doped TiO_2 particles and mesoporous carbon are firmly together. Figs. 4(c) and (d) showed large areas of parallel fringes and straight through channels at different magnifications of samples NTC1-3.5, indicating that the nanocomposites have an ordered two-dimensional hexagonal structure. From the TEM images, a large number of uniformly sized Nb-doped TiO_2 nanoparticles were uniformly fixed in the amorphous carbon pore wall with a diameter of about 6.7 nm.

Table 2
The elements type and percentage of the two compounds analyzed by EDX

Samples (wt%)	NTC1-3.5	NTC2-15
Ti	6.38	14.28
O	15.62	29.86
C	75.37	50.38
Nb	0.09	0.15

Table 3
The component type and percentage of the two compounds analyzed by XRF

Samples (wt%)	NTC1-3.5	NTC2-15
TiO_2	25.43	40.52
C	72.37	58.38
Nb	0.07	0.11

3.4. X-ray diffraction

The XRD patterns of the mesoporous carbon–niobium doped TiO_2 nanocomposites (NTC1-3.5 and NTC2-15) are shown in Fig. 5. It can be seen from the figure that the 2θ angles of the composites prepared by self-assembly method or sol–gel method show strong diffraction peaks around 25.3°, 38.3°, 48.2°, 54.5° and 62.5°, indexed as 101, 004, 200, 105, 211 and 204 reflections of anatase phase, suggesting a formation of TiO_2 nanocrystals after heated. All the identified peaks for mesoporous carbon–niobium doped TiO_2 nanocomposites were assigned to anatase TiO_2, which was mainly detected in all samples without any contribution of rutile or brookite phase. We also observed that the diffraction peak at the (101) plane of the nanocomposites prepared by self-assembly method is broadened and the diffraction peak of the (101) plane is wider than that of the nanocomposites prepared by sol–gel method. The broadening of the (101) diffraction peak can be attributed to the weak crystallization of the TiO_2 particles [41]. The size of anatase nanocrystals in NTC2-15 and NTC1-3.5 was estimated to be 15.3 and 6.9 nm, respectively, based on the Scherrer formula. The crystallographic difference of the nanocomposites is due to the restriction of mass diffusion between the carbonized phenolic resin and TiO_2 particles, which prevents the crystallization, phase transformation and crystal growth of TiO_2 particles [42].

3.5. Ultraviolet–visible spectrophotometry

The optical properties of the mesoporous carbon–niobium doped TiO_2 nanocomposites were measured by UV–Vis diffuse reflectance spectroscopy. UV–Vis diffuse reflectance spectra of pure C-TiO_2 and Nb-doped C-TiO_2 (0.2% Nb) nanocomposites are shown in Figs. 6 and 7. From Fig. 6 it can be seen that both the pure C-TiO_2 and Nb-doped C-TiO_2 (0.2% Nb) nanocomposites have obvious absorption at 200–360 nm before or after Nb doping, which is caused by the inherent band gap of the excited electron transition of TiO_2 photocatalyst. When the wavelength moves from 400 to 700 nm in the visible region, the absorption of the pure C-TiO_2 is significantly reduced in contrast to the existence of a certain degree of absorption of Nb-doped C-TiO_2. The main reason is that the Nb ions interrupt into the lattice of C-TiO_2 nanocomposites then import an intermediate level between the conduction band and the valence band formed of C-TiO_2 nanocomposites. The photogenerated electrons can be transited to the intermediate energy level first and then transited to the conduction band of Nb-doped C-TiO_2 nanocomposites so the required excitation energy can be reduced to the range of visible light and the Nb-doped C-TiO_2 nanocomposites has certain visible light absorption properties [43].

In order to calculate the forbidden band width of C-TiO_2 nanocomposites before and after doping, we make a curve about the forbidden band width adopted the modified Kubelka–Munk formula [44,45], with $h\nu = 1{,}240.7/\lambda$ as the

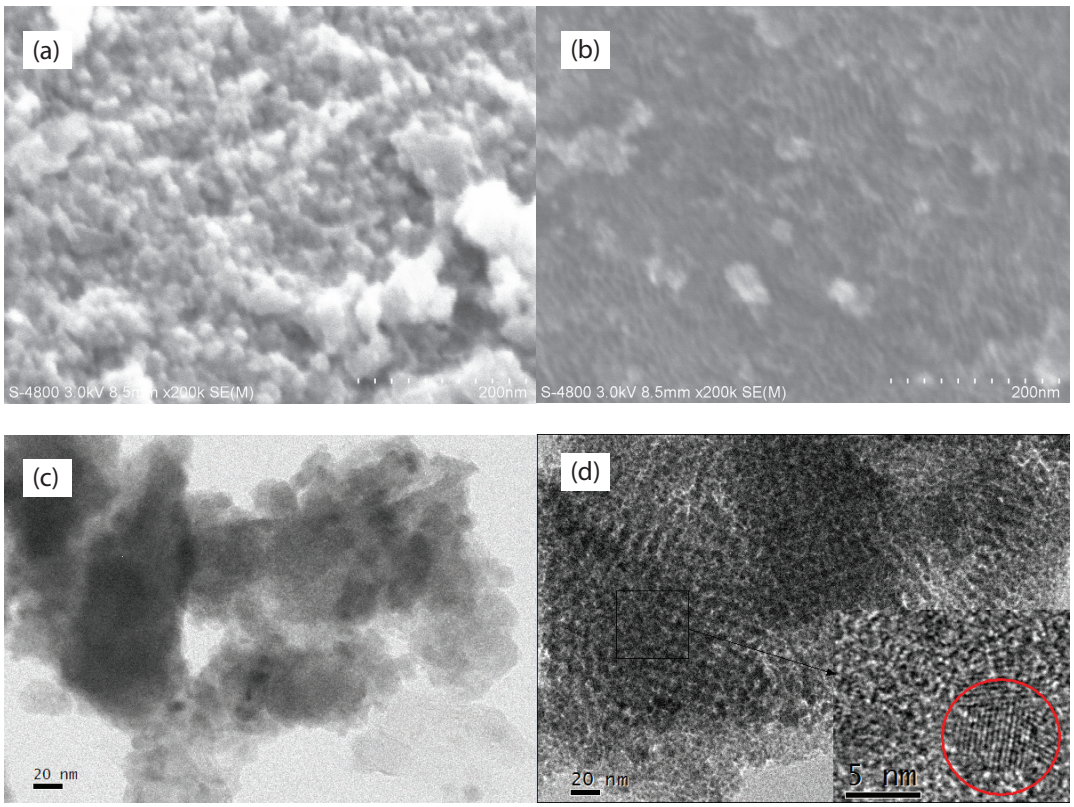

Fig. 4. SEM images of mesoporous carbon–niobium doped TiO_2 nanocomposites of (a) NTC2-15, (b) NTC1-3.5 and the TEM images of mesoporous carbon–niobium doped TiO_2 nanocomposites of (c) NTC2-15 under 20 nm, (d) NTC1-3.5 under 20 nm.

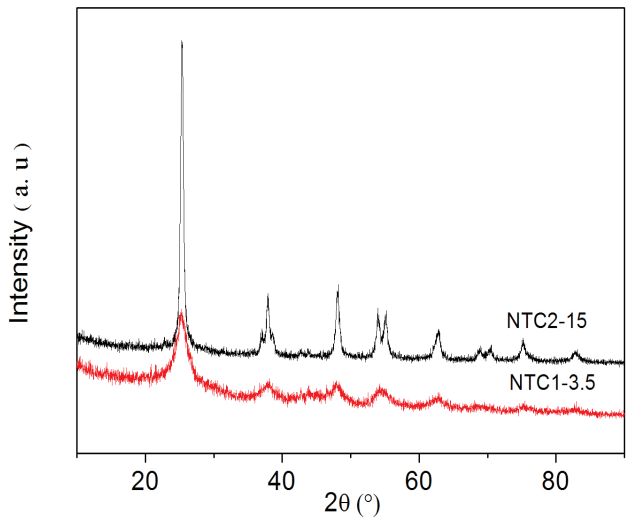

Fig. 5. XRD patterns of mesoporous carbon–niobium doped TiO_2 nanocomposites.

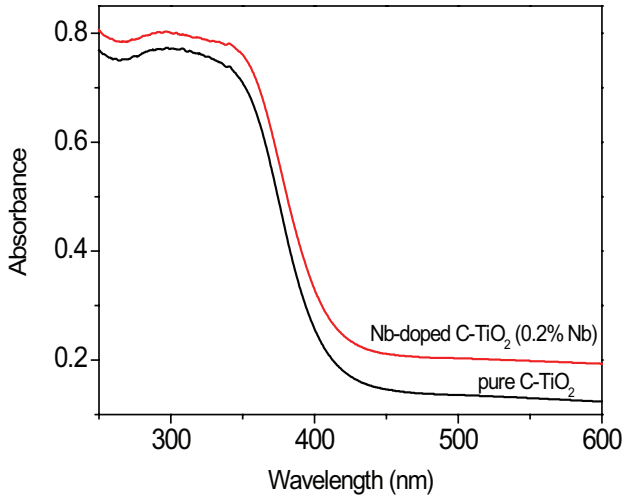

Fig. 6. UV–Vis diffuse reflectance spectra of pure C-TiO_2 and Nb-doped C-TiO_2 (0.2% Nb) nanocomposites.

abscissa and $(A hv)^{1/2}$ as the ordinate and then make the tangential method to find the material band gap width of the materials seen in Fig. 7. It can be seen from Fig. 7 that the band gap of pure C-TiO_2 and Nb-doped C-TiO_2 nanocomposites is around 3.13 and 3.04 eV, respectively. It shows that the band gap of the C-TiO_2 nanocomposites doped with niobium ion is reduced compared with the pure C-TiO_2 particles, which means that the absorption range of Nb-doped C-TiO_2 nanocomposites is higher than that of pure C-TiO_2 particles and it has a certain photocatalytic activity in the larger wavelength range.

3.6. X-ray photoelectron spectroscopy

The XPS test results of the nanocomposites prepared by the self-assembly and sol–gel methods are shown in Fig. 8.

In the scanning range of 0–1,300 eV, it can be seen that C1s, Ti2p and O1s peaks appeared evident in the sample, that is, there are C, Ti and O elements in the sample. In addition, there is Nb3d peak in the material although the signal of this peak is weak due to its low mass concentration in the nanocomposites and it can explain that the Nb element is successfully doped into the nanocomposite. The carbon and oxygen elements in NTC1-3.5 are relatively large and the proportion of titanium and niobium is 5.99% and 0.07%, respectively. Similarly, the proportion of carbon and oxygen in NTC2-15 is larger and the proportion of titanium and niobium is 13.31% and 0.12%, respectively. Because of the different doping amount of Nb element, the XPS results show that the Nb content in NTC2-15 is higher than NTC1-3.5.

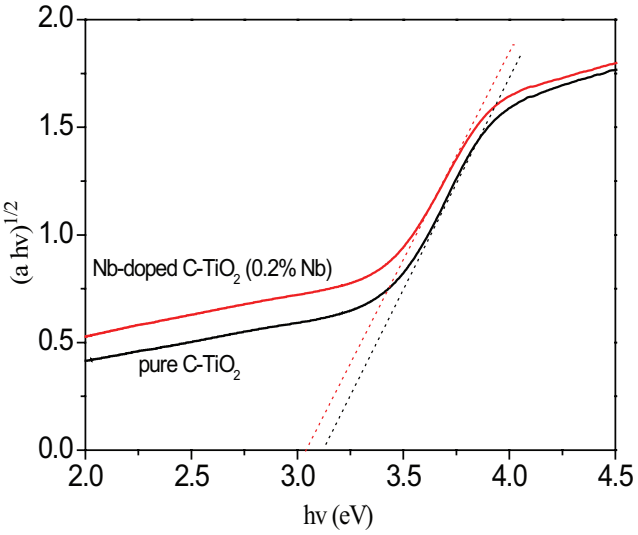

Fig. 7. The modified Kubelk–Munk function of pure C-TiO_2 and Nb-doped C-TiO_2 (0.2% Nb) nanocomposites.

In the XPS spectra test of samples NTC1-3.5 and NTC2-15, both the $Ti2p_{3/2}$ and $Ti2p_{1/2}$ peaks (at 459.5 and 465.3 eV, respectively) appeared in Fig. 8(b) and the peaks are in the standard symmetrical shape. Metal (Nb^{5+}) and nonmetallic elements (C) were co-doped into the TiO_2 lattice, which caused the shift of characteristic peaks about 1 eV to the high binding energy direction compared with the XPS manual peak data of TiO_2. Fig. 8(c) shows the XPS spectrum of the C1s and the peak at 284.6 eV is the characteristic peak of the free carbon. Another two weak shoulders appear in the spectrum at 286.5 and 288.5 eV, represented C–O and C=O, indicating the existence of Ti–O–C bonds which means that the carbon element does exist doping on the TiO_2 lattice [46]. In the nanocomposites, the carbon element mainly exists in two forms: the majority of carbon exits as free carbon in the form of residual on the surface of TiO_2, causing the absorption ability of nanocomposites in the visible region and playing a role in photosensitization of the photocatalytic reaction. A small fraction of carbon is doped into the lattice of TiO_2 that forms a doping level in the middle of the TiO_2 band gap and

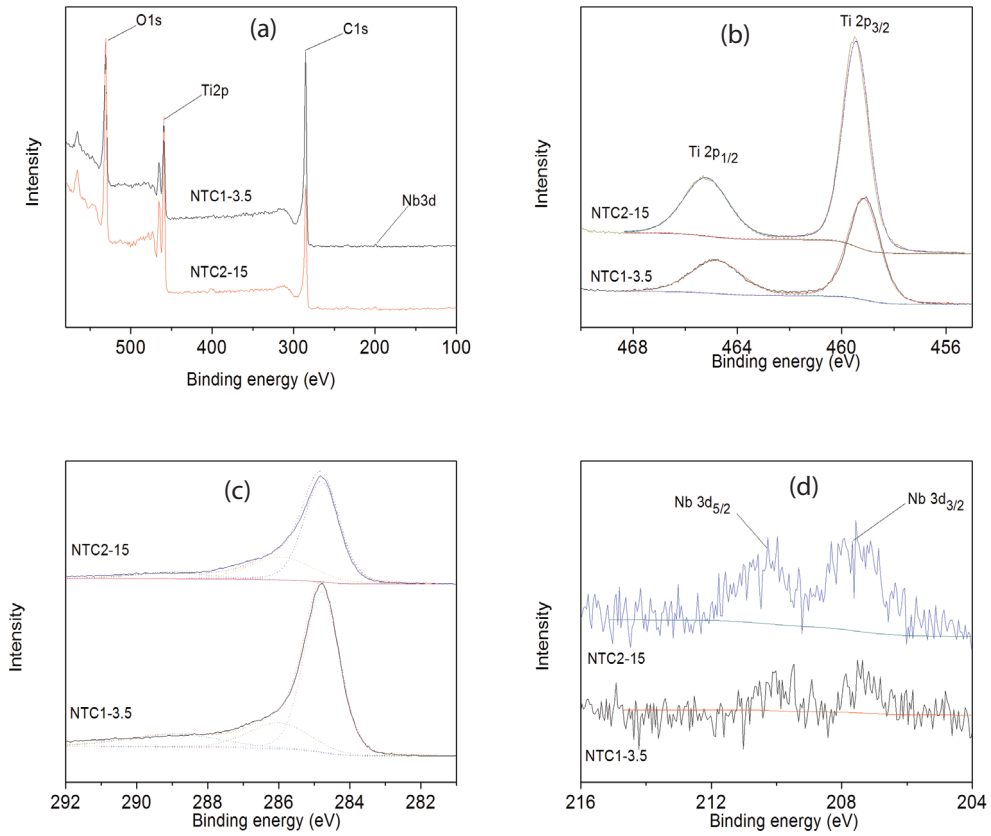

Fig. 8. XPS spectra of NTC1-3.5 and NTC2-15: (a) Full-spectrum, (b)Ti2p, (c) C1s and (d) Nb3d.

narrows the band gap. Fig. 8(d) shows the single spectrum of Nb3d and we can see that the peaks of $Nb3d_{5/2}$ and $Nb3d_{3/2}$ exit at 207.2 and 210.3 eV, respectively. The binding energies of $Nb3d_{5/2}$ and $Nb3d_{3/2}$ in Nb_2O_5 are very close to 207.4 and 210.5 eV, respectively, in comparison with the control standard spectra which indicate that the Nb element is in the form of Nb^{5+} in the mesoporous carbon–niobium doped TiO_2 nanocomposites.

3.7. Adsorption and photocatalytic activity

The adsorption and photocatalytic performance of mesoporous carbon–niobium doped TiO_2 nanocomposites was evaluated by the methylene blue degradation under darkness and UV irradiation at room temperature. The results of the treatment of the methylene blue solution were evaluated using the NTC1-a nanocomposites synthesis by self-assembled method seen in Fig. 9. First, the experiment proceeds in the darkness for 6 h, then at zero-time, under the UV light for photocatalytic degradation. The adsorption of the methylene blue by NTC1-a nanocomposites has been basically reached equilibrium for 6 h after the reaction, so we set the dark reaction time to 6 h. It was found that the adsorption capacities of NTC1-14, NTC1-7, NTC1-3.5 and NTC1-1.75 composites were increasing because the carbon content of this nanocomposites is gradually increased. The removal rates of methylene blue were 13.75%, 41.43%, 57.38% 80.57%, respectively, after the adsorption equilibrium was reached. After adsorption equilibrium, the concentration of methylene blue solution was 43.13, 29.29, 21.31, 9.72 mg/L. After photocatalysis, the concentration was reduced to 38.87, 26.79, 18.03, 5.80 mg/L. It can be found that the photocatalytic degradation of methylene blue was very limited after 3.5 h UV irradiation, which was not worth mentioning compared with methylene blue removed by dark reaction adsorption. The photocatalytic activity was poor in the nanocomposites no matter with high TiO_2 content or high mesoporous carbon content. However, the XRD, XPS and TEM characterizations indicate that there is anatase-type TiO_2 in the NTC1-a nanocomposites. It can be concluded that the TiO_2 particles are coated with mesoporous carbon in the pore walls of the NTC1-a nanocomposites synthesis by self-assembled method. Hence, there is small part of the TiO_2 directly exposed to the surface of the nanocomposites, while the TiO_2 photodegradation process is occurring in the surface. Therefore, the photocatalytic capacity of NTC1-a nanocomposites is greatly restricted on the surface of the TiO_2 particles.

At the same time, the results of the treatment of the methylene blue solution were evaluated using the NTC2-b nanocomposites synthesis by sol–gel method seen in Fig. 10. The nanocomposites prepared by the sol–gel method not only have good adsorption ability, but also have good photodegradation ability. After adsorption equilibrium, the concentration of methylene blue solution was 49.80, 41.40, 36.96, 33.39, 26.35 mg/L. After photocatalysis, the concentration was reduced to 24.98, 15.36, 10.30, 5.48, 14.48 mg/L. The dye removal by adsorption stage were 0.40%, 17.20%, 26.08%, 33.22%, 47.30%, respectively. In the case of NTC2-15, the total removal rate of methylene blue after adsorption and photocatalysis was about 89.23%, of which 32.67% methylene blue

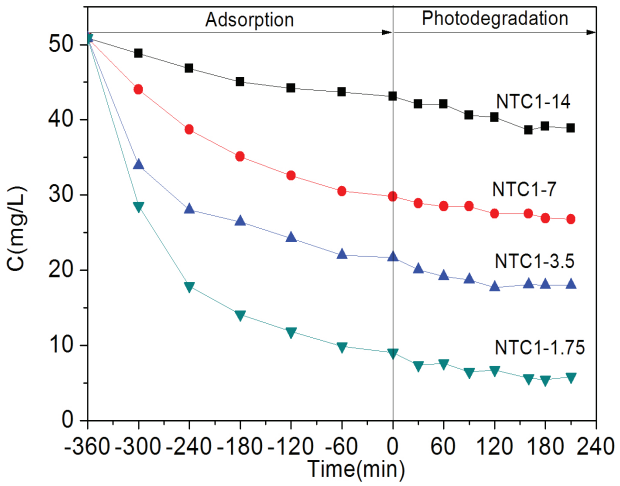

Fig. 9. Adsorption–photodegradation for MB on NTC1-a composites.

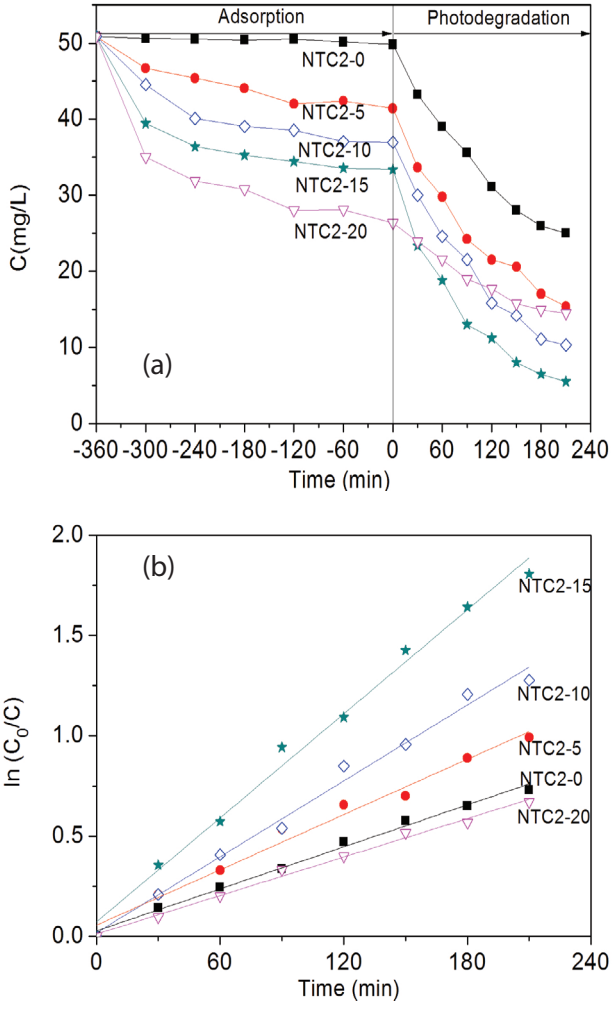

Fig. 10. (a) Adsorption–photodegradation for MB on NTC2-b nanocomposites and (b) photocatalytic degradation of MB follows pseudo-first-order kinetics.

was removed by adsorption and the last 56.56% was removed by photocatalytic degradation.

The adsorption and photocatalytic properties of the nanocomposites are significantly affected by the carbon content of the composite materials. The adsorption process of NTC2-b nanocomposites is similar to that of NTC1-a and the equilibrium adsorption can be achieved in about 6 h. The adsorption ability of methylene blue is increased with the increase of carbon content in the nanocomposites. The photocatalytic degradation of methylene blue follows a pseudo-first-order kinetics (shown in Fig. 10(b)). Among the prepared nanocomposites, NTC2-15 nanocomposite (k = 0.072 min^{-1}) exhibited the highest rate of degradation of methylene blue, followed by NTC2-10 (k = 0.055 min^{-1}), NTC2-5 (k = 0.027 min^{-1}), NTC2-0 (k = 0.018 min^{-1}) and NTC2-20 (k = 0.011 min^{-1}). The results show that the NTC2-15 exhibits the highest photocatalytic activity and complete degradation of methylene blue within 3.5 h. In contrast, the photocatalytic activity of NTC2-0 is low and almost 49.1% methylene blue remains within the same 3.5 h of irradiation. Under the appropriate amount of doping, it was found that the increase in mesoporous carbon concentration in nanocomposites, enhanced photocatalytic activity up to a certain extent, which is attributed to the high adsorption performance of the methylene blue and the high mobility of the photogenerated electrons on the surface of NTC2-b nanocomposites. The adsorption ability of organic substances on the surface of photocatalyst is an important factor affecting the efficiency of photolysis. It can accumulate more organic substances on the surface of catalyst with addition of photocatalyst to effective adsorbent, resulting in the local increase of organic concentration on the surface of Nb-TiO_2. Then it can increase the transfer rate of interfacial charges and reduce the recombination rate between holes and electrons thus improving the photodegradation rate. However, excessive amount of mesoporous carbon would retard the photocatalytic performance of the nanocomposites. Excessive mesoporous carbon loading could have increased the probability of collision between electrons and holes, thus promoting recombination of photogenerated electron–hole pairs then ultimately lower the photocatalytic performance of the nanocomposites [47]. The higher mesoporous carbon content resulted in low photocatalytic degradation of methylene blue compared with the NTC2-15, which may be due to the blocking of UV light and excess mesoporous carbon acts as the adsorption centers during photocatalytic process [48]. The photocatalytic degradation was in the order of NTC2-15 > NTC2-10 > NTC2-5 > NT > NTC2-20. The concentration of TOC in the methylene blue solution was examined in order to show that the methylene blue solution is absorbed and degraded by the composite rather than decolorization. From Fig. 11, it can be seen that the decrease trend of TOC concentration is similar to the decrease trend of methylene blue (MB) concentration, which indicates that MB is adsorbed and degraded rather than decolor. Therefore, the concentration of MB is used to represent the properties of composite.

In addition, the photodegradation of methylene blue was monitored for four consecutive cycles using NTC2-15 compared with NTC2-0. Fig. 12 shows that both the degradation ability of the two materials is high in the first photodegradation but the degradation rate of the NTC2-15 is higher than that of the NTC2-0 nanocomposites. The degradation ability of NTC2-0 is gradually reduced after multiple cycles with the so-called catalyst poisoning appears. It was found that NTC2-0 showed a deep blue color after several cycles, that is, much methylene blue gathered on the surface of the NTC2-0 nanocomposites. As known, the photocatalytic process occurs mainly on the surface of the catalyst. Therefore, the photodegradation ability of the NTC2-0 nanocomposites is affected by the fact that a lot of dye molecules accumulated on the surface of the nanocomposites which has no time to degrade, thus the degradation effect reduced rapidly with the increase in the number of cycles. However, NTC2-15 showed no obvious degradation after four cycles because the methylene blue molecules in the solution were preferentially adsorbed on the mesoporous carbon and then the methylene blue molecules were photodegraded with transferring to the surface of TiO_2. It can be seen that the addition of mesoporous carbon significantly improves the recycle capacity of the material.

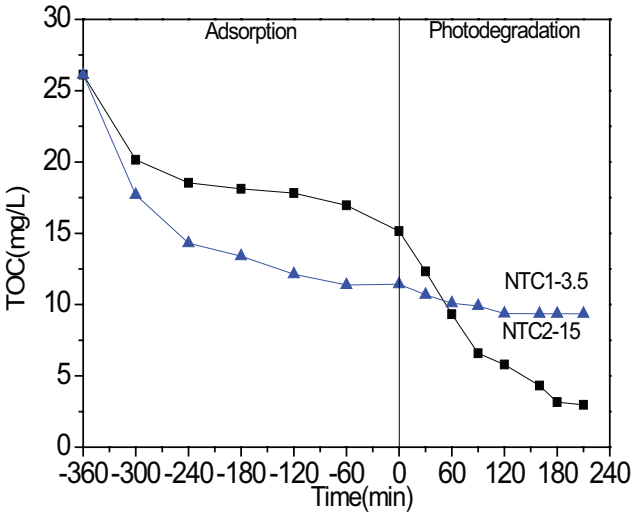

Fig. 11. Adsorption–photodegradation for TOC concentration of MB solution on NTC1-3.5 and NTC2-15 composites.

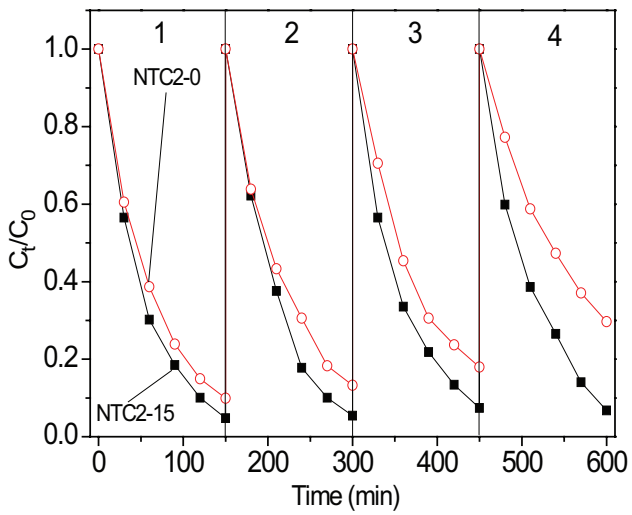

Fig. 12. Cyclic photodegradation for MB on NTC2-15 and NTC2-0.

The photodegradation rate of NTC2-15 remains constant during the four consecutive cycles, indicating that the photocatalyst is stable under UV light irradiation. The photocatalyst showed 100% reusability after four times of recycling.

In order to further investigate the influence of pH and catalyst mass *n* on the removal rate of MB, NTC1-3.5 and NTC2-15 nanocomposites were selected to discuss their total removal rate after adsorption and photodegradation of MB solution, which are shown in Fig. 13.

From Fig. 13, it can be seen that the removal rate of methylene blue tends to be stable when the pH value is higher than 6 after the adsorption and photodegradation of composite materials for 50 mg/L methylene blue solution. This is because the degree of molecular is higher under acidic conditions. The adsorption amount of the composite materials to the non-dissociative state is smaller than that of the dissociative state, so the treatment effect of the composite materials is poor under acidic conditions. With the increase of catalyst mass, the removal rate of methylene blue is higher and higher. However, the removal rate of methylene blue is very high and the excessive addition of composite material will lead to a decrease in the amount of saturated adsorption when the dosage is higher than 0.5.

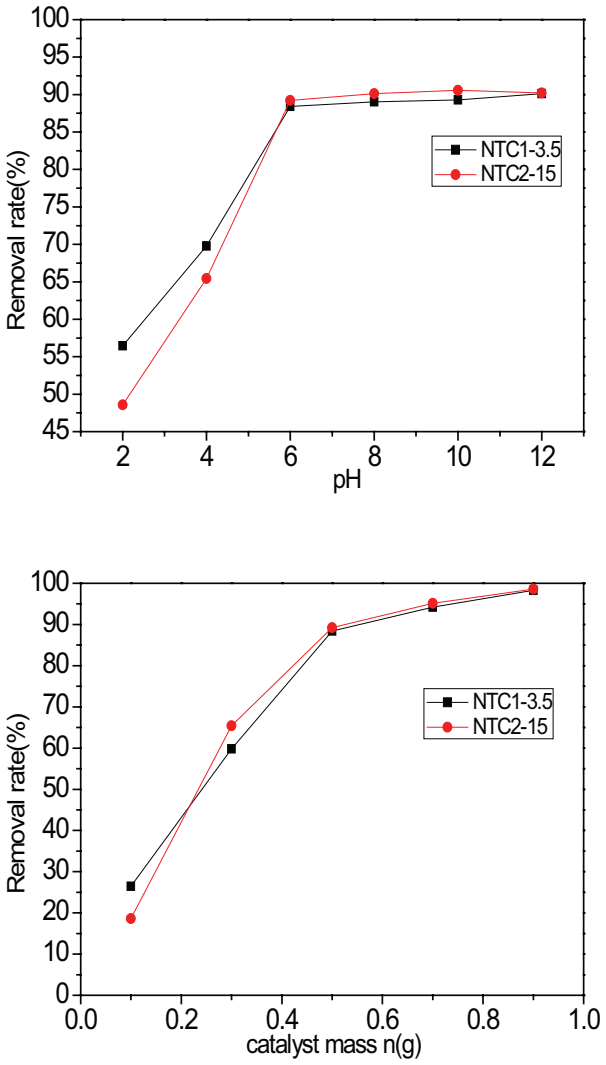

Fig. 13. Effect of pH and catalyst mass *n* on removal rates of MB on NTC1-3.5 and NTC2-15 composites.

4. Conclusions

The mesoporous carbon–niobium doped TiO_2 nanocomposites via the self-assembly and sol–gel methods were successfully prepared without affecting the TiO_2 structure. The existence of mesoporous carbon and niobium element was confirmed by XRD, XPS, TEM, SEM and UV–Vis spectroscopy analysis. From the UV–Vis spectroscopy test, we investigate that the extension effect of Nb-doped TiO_2 nanocomposite about the optical absorption into the visible assuredly appeared and utilized a larger portion of the sunlight. The microstructure analysis indicated that the anatase TiO_2 particles are uniformly dispersed on mesoporous carbon sheets in the prepared nanocomposites. The results demonstrated that the existence of mesoporous carbon enhanced the photocatalytic degradation of methylene blue. The apparent photocatalytic reaction rate constant of NTC2-15 nanocomposite is about four times higher than that of pure Nb-TiO_2 particles. Especially, the NTC2-15 exhibits high photocatalytic activity compared with pure Nb-TiO_2 under UV light, likely due to the appropriate adsorption ability and effective separation of photogenerated charges. Although NTC1-a nanocomposites have a strong adsorption performance, it does not play an ideal photocatalytic effect. However, NTC2-b nanocomposites not only show good adsorption effect but also play a better photocatalytic degradation effect. The photocatalytic effect of NTC2-15 is best when the mass content of mesoporous carbon is 15% and NTC2-15 shows a good ability in cyclic photodegradation by a more in-depth experimental study.

Acknowledgments

Financial support for this research was provided by the Operational Funds for the Central Universities, China (Grant no. 2016B04614), the National Key Scientific Instrument and Equipment Development Project (Grant No. 2014YQ060773), Project 948: the water detection system trace volatile organic compounds (30155045912), ordinary university graduate student innovation projects, Jiangsu, 2015 (KYZZ15_0147), Research and Demonstration on the Key Technology of Resourceized and Harmless Treatment of Industrial Waste Salt (Grant No. 20165043212), the Key Natural Science Foundation, transformation mechanism and control principle of nitrogenous pollutant in the urban water supply system (Grant No. 51438006), the Priority Academic Program Development of Jiangsu Higher Education Institutions.

References

[1] U. Pal, A. Sandoval, S.I. Madrid, G. Corro, V. Sharma, P. Mohanty, Mixed titanium, silicon, and aluminum oxide nanostructures as novel adsorbent for removal of rhodamine 6G and methylene blue as cationic dyes from aqueous solution, Chemosphere, 163 (2016) 142–152.

[2] M. Das, K.G. Bhattacharyya. Use of raw and acid-treated MnO_2 as catalysts for oxidation of dyes in water: a case study with aqueous methylene blue, Chem. Eng. Commun., 202 (2015) 1375696091.

[3] S. Agarwal, H. Sadegh, M. Monajjemi, A.S. Hamdy, G.A.M. Ali, A.O.H. Memar, R. Shahryari-Ghoshekandi, I. Tyagi, V.K. Gupta, Efficient removal of toxic bromothymol blue and methylene blue from wastewater by polyvinyl alcohol, J. Mol. Liq., 218 (2016) 191–197.
[4] A.H.A. Dabwan, N. Yuki, N.A.M. Asri, H. Katsumata, T. Suzuki, S. Kaneco, Removal of methylene blue, rhodamine B and ammonium ion from aqueous solution by adsorption onto sintering porous materials prepared from coconut husk waste, Open J. Inorg. Non-metal. Mater., 5 (2015) 21–30.
[5] M.J. Andritsos, Con: Methylene Blue should not be used routinely for vasoplegia perioperatively, J. Cardiothor. Vasc. Anesth., 25 (2011) 739–743.
[6] T.S. Ahmed, Methylene blue toxicity following infusion to localize parathyroid adenoma, J. Laryngol. Otol., 120 (2006) 138–140.
[7] S.K. Sharma, 11. Hen Feather: A Remarkable Adsorbent for Dye Removal, John Wiley & Sons, Inc., 2015.
[8] J. Fu, Z. Chen, M. Wang, S. Liu, J. Zhang, J. Zhang, R. Han, Q. Xu, Adsorption of methylene blue by a high-efficiency adsorbent (polydopamine microspheres): kinetics, isotherm, thermodynamics and mechanism analysis, Chem. Eng. J., 259 (2015) 53–61.
[9] A. Mittal, M. Teotia, R.K. Soni, J. Mittal, Applications of egg shell and egg shell membrane as adsorbents: a review, J. Mol. Liq., 223 (2016) 376–387.
[10] J. Jimenez-Villarin, A. Serra-Clusellas, C. Martínez, A. Conesa, J. Garcia-Montaño, E. Moyano, Liquid chromatography coupled to tandem and high resolution mass spectrometry for the characterisation of ofloxacin transformation products after titanium dioxide photocatalysis, J. Chromatogr. A., 1443 (2016) 201–210.
[11] K.R. Reddy, M. Hassan, V.G. Gomes, Hybrid nanostructures based on titanium dioxide for enhanced photocatalysis, Appl. Catal., A, 489 (2015) 1–16.
[12] L. Li, J. Yan, T. Wang, Z.J. Zhao, J. Zhang, J. Gong, N. Guan, Sub-10 nm rutile titanium dioxide nanoparticles for efficient visible-light-driven photocatalytic hydrogen production, Nat. Commun., 6 (2015) 5881.
[13] P. Fernández-Ibáñez, M.I. Polo-López, S. Malato, S. Wadhwa, J.W.J. Hamilton, P.S.M. Dunlop, R.D. Sa, E. Magee, K.O. Shea, D.D. Dionysiou, Solar photocatalytic disinfection of water using titanium dioxide graphene composites, Chem. Eng. J., 261 (2015) 36–44.
[14] R. Li, Y. Weng, X. Zhou, X. Wang, Y. Mi, R. Chong, H. Han, C. Li, Achieving overall water splitting using titanium dioxide-based photocatalysts of different phases, Energy Environ. Sci., 8 (2015) 2377–2382.
[15] A.N. Wang, Y. Teng, X.F. Hu, L.H. Wu, Y.J. Huang, Y.M. Luo, P. Christie, Diphenylarsinic acid contaminated soil remediation by titanium dioxide (P25) photocatalysis: degradation pathway, optimization of operating parameters and effects of soil properties, Sci. Total Environ., 541 (2016) 348.
[16] Y. Meng, Y. Wang, Q. Han, N. Xue, Y. Sun, B. Gao, Q. Li, Trihalomethane (THM) formation from synergic disinfection of biologically treated municipal wastewater: effect of ultraviolet (UV) irradiation and titanium dioxide photocatalysis on dissolve organic matter fractions, Chem. Eng. J., 303 (2016) 252–260.
[17] D. Dolat, S. Mozia, R.J. Wróbel, D. Moszyński, B. Ohtani, N. Guskos, A.W. Morawski, Nitrogen-doped, metal-modified rutile titanium dioxide as photocatalysts for water remediation, Appl. Catal., B, 162 (2015) 310–318.
[18] R. Sadowski, M. Strus, M. Buchalska, P.B. Heczko, W. Macyk, Visible light induced photocatalytic inactivation of bacteria by modified titanium dioxide films on organic polymers, Photochem. Photobiol. Sci., 14 (2015) 514.
[19] B. Chládková, E. Evgenidou, L. Kvítek, A. Panáček, R. Zbořil, P. Kovář, D. Lambropoulou, Adsorption and photocatalysis of nanocrystalline TiO_2 particles for Reactive Red 195 removal: effect of humic acids, anions and scavengers, Environ. Sci. Pollut. Res., 22 (2015) 16514–16524.
[20] M.C. Wang, H.J. Lin, T.S. Yang, Characteristics and optical properties of iron ion (Fe^{3+})-doped titanium oxide thin films prepared by a sol–gel spin coating, J. Alloys Comp., 473 (2009) 394–400.
[21] Q.R. Deng, X.H. Xia, M.L. Guo, Y. Gao, G. Shao, Mn-doped TiO_2 nanopowders with remarkable visible light photocatalytic activity, Mater. Lett., 65 (2011) 2051–2054.
[22] H. Huang, H. Huang, Z. Lu, H. Peng, X. Ye, D.Y.C. Leung, Enhanced degradation of gaseous benzene under vacuum ultraviolet (VUV) irradiation over TiO_2 modified by transition metals, Chem. Eng. J., 259 (2015) 534–541.
[23] M.R. Hoffmann, S.T. Martin, W. Choi, D.W. Bahnemann, Environmental applications of semiconductor photocatalysis, Chem. Rev., 95 (1995) 69–96.
[24] Y. Hou, X. Wang, L. Wu, A. Zhengxin Ding, X. Fu, Efficient decomposition of benzene over a β-Ga_2O_3 photocatalyst under ambient conditions, Environ. Sci. Technol., 40 (2006) 5799.
[25] R. Raccichini, A. Varzi, S. Passerini, B. Scrosati, The role of graphene for electrochemical energy storage, Nat. Mater., 14 (2015) 271.
[26] F. Perreault, D.F.A. Fonseca, M. Elimelech, Environmental applications of graphene-based nanomaterials, Chem. Soc. Rev., 46 (2015) 5861.
[27] A.G. Arani, E. Haghparast, Z.K. Maraghi, S. Amir, Static stress analysis of carbon nanotube reinforced composite (CNTRC) cylinder under non-axisymmetric thermo-mechanical loads and uniform electro-magnetic fields, Composites Part B., 68 (2015) 136–145.
[28] S.S.C.S. Sahu, A comparative study on heat transfer enhancement of low volume concentration of Al_2O_3-water and CNT-water nanofluids in laminar regime using helical screw tape inserts, Chem. Eng. Process. Process Intensif., 88 (2014) 78–88.
[29] C. Chung, Y.K. Kim, D. Shin, S.R. Ryoo, B.H. Hong, D.H. Min. Biomedical applications of graphene and graphene oxide, Accounts Chem. Res., 46 (2013) 2211.
[30] V. Štengl, D. Popelková, P. Vláčil. TiO_2–graphene nanocomposite as high performance photocatalysts, J. Phys. Chem. C., 115 (2011) 25209–25218.
[31] M. Naushad, A. Mittal, M. Rathore, V. Gupta, Ion-exchange kinetic studies for Cd(II), Co(II), Cu(II), and Pb(II) metal ions over a composite cation exchanger, Desal. Wat. Treat., 54 (2015) 2883–2890.
[32] A. Mittal, R. Ahmad, I. Hasan, Iron oxide-impregnated dextrin nanocomposite: synthesis and its application for the biosorption of Cr(VI) ions from aqueous solution, Desal. Wat. Treat., 57 (2016) 15133–15145.
[33] H. Zhang, P. Xu, G. Du, Z. Chen, K. Oh, D. Pan, Z. Jiao, A facile one-step synthesis of TiO_2/graphene composites for photodegradation of methyl orange, Nano Res., 4 (2011) 274–283.
[34] Y. Zhang, Z.R. Tang, X. Fu, Y.J. Xu, TiO_2-graphene nanocomposites for gas-phase photocatalytic degradation of volatile aromatic pollutant: is TiO_2-graphene truly different from other TiO_2-carbon composite materials? ACS Nano., 4 (2010) 7303–7314.
[35] W. Fan, Q. Lai, Q. Zhang, Y. Wang, Nanocomposites of TiO_2 and reduced graphene oxide as efficient photocatalysts for hydrogen evolution, J. Phys. Chem. C., 115 (2011) 10694–10701.
[36] J.S. Lee, K.H. You, C.B. Park, Highly photoactive, low bandgap TiO_2 nanoparticles wrapped by graphene. Adv. Mater., 24 (2012) 1084.
[37] J. Zhong, J. Wang, L. Tao, M. Gong, L. Zhimin, Y. Chen, Photocatalytic degradation of gaseous benzene over TiO_2/Sr_2CeO_4: kinetic model and degradation mechanisms, J. Hazard. Mater., 139 (2007) 323.
[38] Y. Ding, J. Zhu, C. Yang, S. Chen, Adsorption equilibrium, kinetics and thermodynamics of dichloroacetic acid from aqueous solution using mesoporous carbon, Environ. Technol., 35 (2014) 1962.
[39] Y. Ding, J. Zhu, D. Ji, Y. Cao, X. Ling, W. Chen. Enhancing adsorption efficiency of dichloroacetic acid onto mesoporous carbons: procedure optimization, mechanism and characterization, J. Colloid Interface Sci., 452 (2015) 134–140.
[40] K.S. Walton, R.Q. Snurr, Applicability of the BET method for determining surface areas of microporous metal-organic frameworks, J. Am. Chem. Soc., 129 (2007) 8552.

[41] C.H. Cho, D.K. Kim, D.H. Kim, Photocatalytic activity of monodispersed spherical TiO_2 particles with different crystallization routes, J. Am. Ceram. Soc., 86 (2010) 1138–1145.
[42] Y. Liao, X. Wang, Y. Ma, J. Li, T. Wen, L. Jia, Z. Zhong, L. Wang, D. Zhang, New mechanistic insight of low temperature crystallization of anodic TiO_2 nanotube array in water, Cryst. Growth Des., 16 (2016) 1786–1791.
[43] L. Velasco, J. Parra, C. Ania, Phenol adsorption and photo-oxidation on porous carbon/titania composites, Adsorpt. Sci. Technol., 28 (2010) 727–738.
[44] W. Wei, C. Yu, Q. Zhao, G. Li, Y. Wan, Improvement of the visible-light photocatalytic performance of TiO_2 by carbon mesostructures, Chemistry, 19 (2013) 566.
[45] B. Kramer, Electronic structure and optical properties of amorphous germanium and silicon, Phys. Status Solidi, 47 (1971) 501–510.
[46] X.Y. Zhang, H.P. Li, X.L. Cui, Y. Lin, Graphene/TiO_2 nanocomposites: synthesis, characterization and application in hydrogen evolution from water photocatalytic splitting, J. Mater. Chem., 20 (2010) 2801–2806.
[47] W.K. Jo, Y. Won, I. Hwang, R.J. Tayade, Enhanced photocatalytic degradation of aqueous nitrobenzene using graphitic carbon–TiO_2 composites, Ind. Eng. Chem. Res., 53 (2014) 3455–3461.
[48] Y. Liu, C. Xie, J. Li, T. Zou, D. Zeng, New insights into the relationship between photocatalytic activity and photocurrent of TiO_2/WO_3 nanocomposite, Appl. Catal., A, 433–434 (2012) 81–87.